

# Energy analysis and optimization of a small-scale axial flow turbine for Organic Rankine Cycle application

Yohan Engineer<sup>\*</sup>, Ahmed Rezk, Abul Kalam Hossain

Energy and Bioproducts Research Institute (EBRI), College of Engineering and Physical Sciences, Aston University, Birmingham, B4 7ET, UK

## ARTICLE INFO

### Keywords:

Energy Conversion  
Optimization  
ORC system  
Turbine Performance  
Turbine Design

## ABSTRACT

Increasing the cycle efficiency of Organic Rankine Cycles is an important R&D area. In this study, an effort has been made to optimize various parameters related to the axial flow turbine to maximize an ORC's efficiency. First, a numerical model for a small-scale single-stage axial flow turbine was developed and coupled with a 1D model of an existing ORC system. Then, a parametric study was undertaken for the system working under various turbine inlet conditions, such as turbine pressure ratios and working fluids. An optimization study was undertaken for the turbine flow profile using a low computational intensity Artificial Neural Network coupled with Genetic Algorithm optimization. Investigating the turbine losses revealed that the Mach Number is the most influential factor, which depends on the molar mass of the working fluid. Our study revealed that increasing the degree of superheat by up to 200% enhanced the turbine and overall cycle efficiency by 11% and 5%, respectively. Increasing the turbine total-to-static pressure ratio from 3 to 10 improved the turbine and cycle efficiency by up to 41% and 15%, respectively. Optimizing the turbine's flow profile enhanced the overall loss coefficient by 13.7%, the turbine's total-to-static efficiency by 5.2%, and the overall cycle efficiency from 8.78% to 9.02%.

## 1. Introduction

Worldwide, the power generation sector contributes to 60% share of the global CO<sub>2</sub> emissions. The carbon emission causes of global warming that led to profound environmental impacts in the last few decades such as severe flooding, tsunamis, unbalanced marine ecosystems, higher storm surges, and destruction of arable land [1, 2]. Therefore, a mix of energy sources is required to meet the ever-growing energy demand with far less environmental impact. Medium-grade waste heat sources (150 - 250°C) are available in many industrial applications such as reheating furnace exhausts, blast furnaces, drying and baking ovens, reheat furnace coke ovens, glass melting, cooling water from annealing furnaces, and steam boiler exhaust gases [3–7]. These waste heat sources can be used to generate useful energy [7]. Although steam-based Rankine cycles are the most reliable thermal power generation system, they are thermally less efficient if utilizing heat sources below 370°C. Organic Rankine Cycles (ORCs) are a more feasible alternative to utilize medium-grade heat [8]. Whereas the efficiency of steam-based Rankine cycles has attained maturity, ORCs are still under development, as their performance highly depends on heat source temperatures, heat source fluctuations, cycle configuration and expander types and their designs [9].

The ORCs utilize organic fluids of low boiling temperature and a high molecular mass to exploit medium-grade to low-grade heat sources and generate mechanical shaft power by expanding the high enthalpy fluid produced in the boiler in the expander. Axial flow turbines are widely used in ORCs because of their superior reliability, greater scalability with pressure ratios, design simplicity, relatively less wear and tear due to the reduced moving parts, and minimum vibration [10].

Multiple studies investigated the intensification of power conversion efficiency of ORCs working at a given heat source temperature by employing various working fluids [11]. Many such studies assumed a fixed value for the turbine efficiency between (60 - 90 %), primarily because of the complication in determining the turbine losses [12–17]. Numerous studies investigated the implications of the expander performance in ORCs. Song et al. [18] developed a one-dimensional model to correlate the cycle design to the expander efficiency. They concluded that the turbine efficiency significantly impacts selecting the working fluid and the cycle's parametric determination [18]. Hung et al. [8] observed a significant change in the cyclic efficiency by varying the pressure ratio and inlet temperatures in the expander for a given isentropic expansion. White et al. [19] considered the variation of turbine efficiency in optimizing the ORC cyclic efficiency.

There are two main approaches to predict turbine efficiency: direct

<sup>\*</sup> Corresponding author.

E-mail address: [engineyc@aston.ac.uk](mailto:engineyc@aston.ac.uk) (Y. Engineer).

<https://doi.org/10.1016/j.ijft.2021.100119>

Nomenclature			
$b$	Backbone length (m)	$X_{sb}$	Secondary loss
$C$	Fluid velocity(m/s)	$\Delta X_{pse}$	Blade back radius loss
$C_a$	Axial Fluid velocity (m/s)	$\Delta X_{pm}$	Mach number loss increment
$CR$	Contraction ratio		
$D_h$	Hydraulic diameter (m)	<i>Greek</i>	
$F_L$	Lift Parameter	$\alpha$	Metal exit angle (°)
$G$	Loss coefficient	$\eta$	efficiency
$g$	Universal gas constant (J/mol K)	$\gamma$	Adiabatic gas constant
$ks$	Equivalent sand grain roughness ( $\mu\text{m}$ )	$\mu$	Dynamic viscosity (kg/m-s)
$H$	Specific Enthalpy (kJ/kg)	$\varphi$	Flow Coefficient
$LC_m$	Modified lift coefficient	$\Psi$	Load Coefficient
lossincr	Trailing edge loss increment	$\rho$	Density
$M$	Mach number	<i>Subscript</i>	
$Mach_{outisen}$	Outlet isentropic Mach number	$a$	Annulus loss
$MM$	Molar mass (g/mol)	$B$	Blade
$N_{Saspectrat}$	Aspect ratio loss	$det$	determiner
$N_{pi}$	Incidence loss	$Group1$	Group 1 loss
$N_{pr}$	Reynolds Number loss	$in$	inlet
$N_{pt}$	Trailing edge thickness loss	$N$	Nozzle
<i>Power</i>	Work done by turbine (KW)	$p$	Primary loss
$P$	Pressure (Bar)	$s$	Secondary loss
$Re$	Reynolds number	1	Before nozzle
$s$	Pitch (m)	2	Between nozzle and blade
$SS$	sound speed (m/s)	3	After blade
$T$	Temperature (°C)	<i>Abbreviation</i>	
$te$	Trailing edge thickness (m)	ANN	Artificial Neural Network
$thr$	Throat width (m)	CFD	Computational Fluid Dynamics
$u$	Blade velocity (m/s)	GA	Genetic Algorithm
$V$	Relative velocity (m/s)	GWP	Global Warming Potential
$X_{a1}$	Annulus loss	ORC	Organic Rankine Cycle
$X_{pb}$	Profile loss		

and indirect approaches. The direct approach consists of a group of individual losses collated into a loss model [20], while the indirect approach employs non-dimensional parameters such as volume ratio, size parameter, flow coefficient, and load coefficient [19]. These non-dimensional parameters are less reliable for predicting Reynolds number effects & fluid thermodynamic behaviour particularly for cases where geometric similarity is not maintained with the original test profiles or in the case of fluids with lower molecular mass [21]. Soderberg's model was developed in 1949, and one of the first to use the direct approach widely accepted [22]. Lazzaretto et al. [23] employed the indirect approach to undertake an optimization study to maximize the turbine efficiency that considered the volumetric expansion ratio and size parameter as performance predictors. Macchi and Perdichizzi developed correlations between non-dimensional parameters and Axial ORC turbine efficiency based on the direct approach Craig and Cox loss model [21]. The Craig and Cox loss model was developed in 1971 and validated by many researchers [24, 25], still considered a reliable and accurate method for designing modern impulse-bladed axial flow turbines [26, 27].

The degree of superheating and pressure ratio significantly influence the turbine performance, hence the overall cycle operation. The admission of a working fluid at a high degree of superheating to the expander increases the thermodynamic potential across it for a given pressure ratio, thus providing theoretically economical solutions to improve expander power output [28]. Superheating also allows development of ORCs with wet working fluids [29]. However, extracting the additional thermodynamic potential of superheated fluid depends on the fluid flow passage's losses [30]. Lozza [31] proposed expanding the working fluid directly from the saturated condition at the highest

possible pressure to maximize the power output. It was found that this change had minor effects on the variation in turbine efficiency. Yamamoto et al. [32] carried out a parametric study for ORC utilizing HCFC-123 and observed that ORC performance is a strong function of the expander's operation, which led to reselecting the working fluids of low latent heat and saturated inlet conditions. Weiß et al. [33] conducted an experimental study on axial and radial inward small scale ORC turbines. They reported that in the case of the axial turbine, the isentropic efficiency was increased by about 2% when the pressure ratio was changed from 16 to 22; on the other hand, operating at pressure ratios below 14 showed a decrease in the isentropic efficiency by 8%. The steeper change in the isentropic efficiency at low pressure ratio was attributed to compression shocks in the convergent-divergent nozzle section.

Although the mean-line design and CFD modeling approaches are widely used to predict the performance of axial flow turbines, Artificial Neural Network (ANN) is less computationally intensive and more reliable if specifically coupled with global optimization. Oyama et al. [34] employed ANN to optimize the design of a transonic axial flow compressor. Previous studies using ANN for turbine optimization were limited to either profile improvement or cycle efficiency [35, 36]. Rashidi et al. [37] employed ANN coupled with Swarm of Bees to optimize the efficiency of an ORC with regenerative feedwater heaters. Meroni et al. [38] optimized ORC cycle efficiency while considering a variable turbine efficiency by integrating a one-dimensional turbine model with a steady-state thermodynamic cycle model. The authors considered mass flow rate, pressure ratio, and turbine parameters as independent variables. They concluded that the pressure ratio was more impactful on the overall cycle efficiency [38]. Most studies found in the

literature concerned a single optimized solution with fewer details on the influence of individual ORC parameters, specifically for axial flow turbines [39].

Although previous studies highlighted the importance of considering the variation of the turbine efficiency on ORC performance, the influence of the actual axial flow turbine's efficiency on the cyclic performance in small-scale ORC is yet to be understood [40]. Furthermore, most studies have studied turbine efficiency or cycle efficiency, but not simultaneously [35, 36]. Therefore, the present study aims to envisage the cause of the turbine efficiency losses in the small-scale axial flow turbines and their impact on ORC performance. The objectives of the study are: (i) employing the direct loss model of Craig and Cox to imitate a small scale axial flow turbine and integrate it with a 1D model of an existing Rankine cycle, (ii) understanding the influence of turbine inlet flow conditions and total-to-static stage pressure ratio on the turbine and cyclic performance utilizing low, medium and high temperature organic fluids, and (iii) employing ANN deep learning modelling coupled with generic algorithm (GA) global optimization to optimize the turbine flow path and study its influence on the ORC performance.

The range of parametric analysis and employing an objective, computationally efficient predictive model coupled with a global optimizer are the critical contribution of this study. Multiple variations considered explain the relationship between turbine efficiency and working fluid parameters, using a direct-loss approach, rather than conventionally used indirectly loss correlations [21, 41]. It enabled studying the impact of basic thermodynamic working fluid parameters like sound speed, isentropic enthalpy drop and molar mass. The use of ANNs trained by a direct loss model also demonstrates the loss compromise at the less significant moving blade efficiency to improve the more significant nozzle efficiency, hence improve overall turbine isentropic efficiency. This ANN integrated approach for turbine optimization allows a new methodology for cycle level analysis.

## 2. Materials and methods

### 2.1. Working fluids

Six working fluids were investigated: Pentafluoropropane (R245fa), Isobutane (R600), 2,3,3,3-Tetrafluoropropene (R1234yf), 1,3,3,3-Tetrafluoropropene isomers (R1234ze(E), R1234ze(Z)), and trans-1-chloro-3,3,3-trifluoropropene R1233zd(E). R245fa and R600 are the most popular fluids for low-to-medium-grade heat with relatively high specific power throughput owing to their low saturation temperature [42, 43]. They were considered by the study as baseline fluids. R1234yf and R1234ze isomers are emerging alternatives to alleviate the environmental impacts of the existing organic fluids [44]. R1233zd(E) is a drop-in replacement for R245fa with lower Global Warming Potential (GWP) [45].

### 2.2. Turbine losses modeling

In this study, Craig and Cox's model was employed to determine the performance of an existing axial flow turbine [20]. Craig and Cox developed a graphical correlation based on profile and secondary losses obtained from linear cascade tests, mainly derived from testing with compressed air. This was supplemented by loss correlations from previous efforts focused on specific annulus losses [46–49]. The detailed description of Craig & Cox model and the developed. Numerical correlations are provided in Supporting Information.

The model determines two groups of losses: group-1 that includes the nozzle's primary loss, nozzle's secondary loss, nozzle's annulus loss, blade's primary loss, blade's secondary loss, and blade's annulus loss; group-2 that includes nozzle gland leakage loss, balance hole loss, rotor tip leakage loss, lacing wire loss, wetness loss, disc windage loss, and partial admission loss. This study concentrated on group-1 losses to determine the aerodynamic efficiency associated with the flow path

design. Equations 1-5 present the breakdown of nozzles and blades' primary, secondary, and annulus losses based on Craig and Cox's maps fitting [20].

$$G_{pN} = X_{pbN} \times N_{prN} \times N_{piN} \times N_{ptN} + lossincr_N + \Delta X_{PseN} + \Delta X_{pmN} \quad (1)$$

$$G_{sN} = N_{prN} \times N_{SaspectratN} \times X_{sbN} \quad (2)$$

$$G_{pB} = X_{pbB} \times N_{prB} \times N_{piB} + lossincr_B + \Delta X_{PseB} + \Delta X_{pmB} \quad (3)$$

$$G_{sB} = N_{prB} \times N_{SaspectratB} \times X_{sbB} \quad (4)$$

$$G_a = X_{a1} \quad (5)$$

The Profile losses due to the flow deviation ( $X_{pbN}$ ,  $X_{pbB}$ ), Reynold's number losses account for wall friction ( $N_{prN}$ ,  $N_{prB}$ ), incidence loss ( $N_{piN}$ ,  $N_{piB}$ ), and trailing edge thickness loss for the nozzle and blade ( $N_{ptN}$ ,  $N_{ptB}$ ) are combined to evaluate the nozzle and blade primary losses expressed by  $G_{pN}$  and  $G_{pB}$ .  $lossincr_N$  and  $lossincr_B$  define the additional loss increment due to trailing edge loss for the nozzle and blade. Profile losses due to blade back radius were considered by  $\Delta X_{PseN}$  and  $\Delta X_{PseB}$ .  $\Delta X_{pmN}$  and  $\Delta X_{pmB}$  factor additional losses for supersonic flow with convergent blading. The combined secondary loss factors ( $G_{sN}$  and  $G_{sB}$ ) are a function of the secondary loss factors ( $X_{sbN}$  and  $X_{sbB}$ ) and secondary loss due to aspect ratio ( $N_{SaspectratN}$  and  $N_{SaspectratB}$ ). The total auxiliary loss ( $G_a$ ) is a function of annulus loss  $X_{a1}$ . Equations 6-7 show the blade losses [20]:

$$G_{Group1N} = \frac{G_{pN} + G_{sN} + G_a}{200} \quad (6)$$

$$G_{Group1B} = \frac{G_{pB} + G_{sB} + G_a \times \left(\frac{C_2}{V_2^2}\right)}{200} \quad (7)$$

Group 1 losses for the nozzle and blade are the summation of  $G_{Group1N}$  and  $G_{Group1B}$ . The incidence losses ( $N_{piN}$  and  $N_{piB}$ ) were not considered in this study.

### 2.3. Cycle modelling & assumptions

The T-S diagram and Basic components of the superheated ORC cycle are shown as in Fig. 1(a) and 1(b) respectively. An industrial boiler's flue gas stack was considered as the heat source. The heat source stack mean temperature of 170°C was considered [50]. The heat input  $Q_{in}$  to the Boiler was stated as in equation 9.  $Q_{out}$  is the rejected heat from the system by a water-cooled surface condenser and operates at 30°C mean temperature, as shown in equation 11. Work done ( $W_m$ ) and efficiency ( $\eta_T$ ) of the turbine were quantified using equations 8 and 10. Cycle efficiency was quantified as in equation 12.

$$W_m = \frac{\dot{m} \times (P_1 - P_7)}{\eta_P} \quad (8)$$

$$Q_{in} = -\dot{m}(h_4 - h_1) \quad (9)$$

$$\eta_T = (1 - (G_{Group1N} + G_{Group1B})) \quad (10)$$

$$Q_{out} = \dot{m}(h_5 - h_7) \quad (11)$$

$$\eta_{Cycle} = \frac{W_T - W_P}{Q_{in}} = \frac{\dot{m} \times ((h_4 - h_5) - (h_1 - h_7))}{Q_{in}} \quad (12)$$

The study was limited to subcritical cycles. The heat source and sink temperatures were assumed as constant. Pinch point for the heat source was considered as 10°C [51, 52]. The pinch point for the heat sink was considered as 5°C [53]. As the turbine was assumed to operate at the design point, off design losses were ignored. Profile trailing edge thickness was maintained as 0.3mm, considering limitations within the

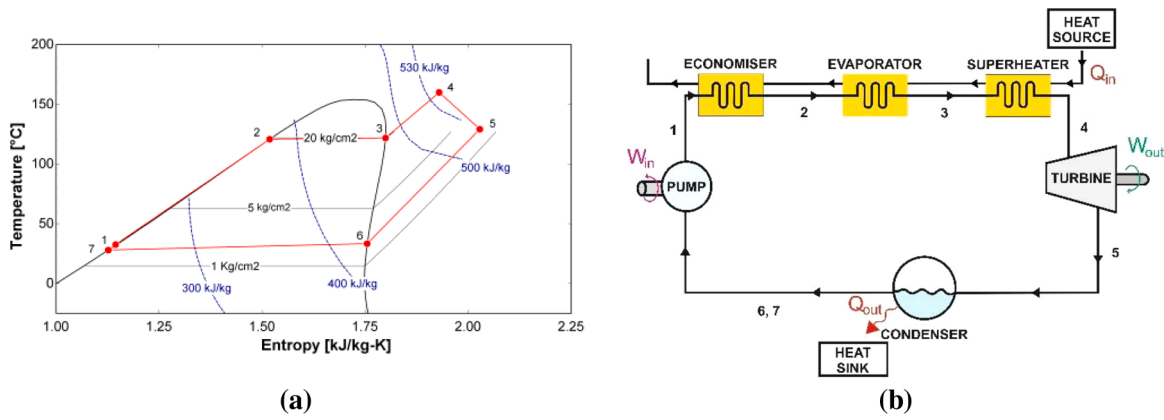


Fig. 1. (a) T-S diagram of superheated ORC for R245fa, (b) components of a superheated ORC

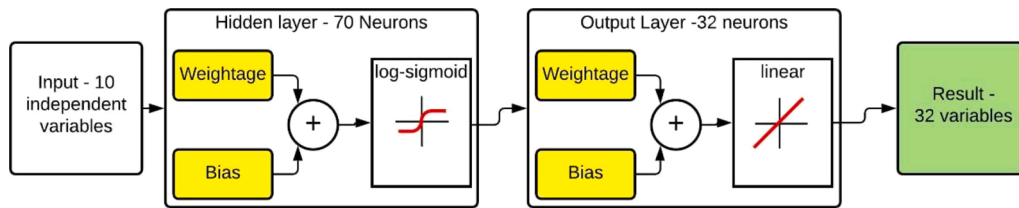


Fig. 2. The architecture of Artificial Neural Network

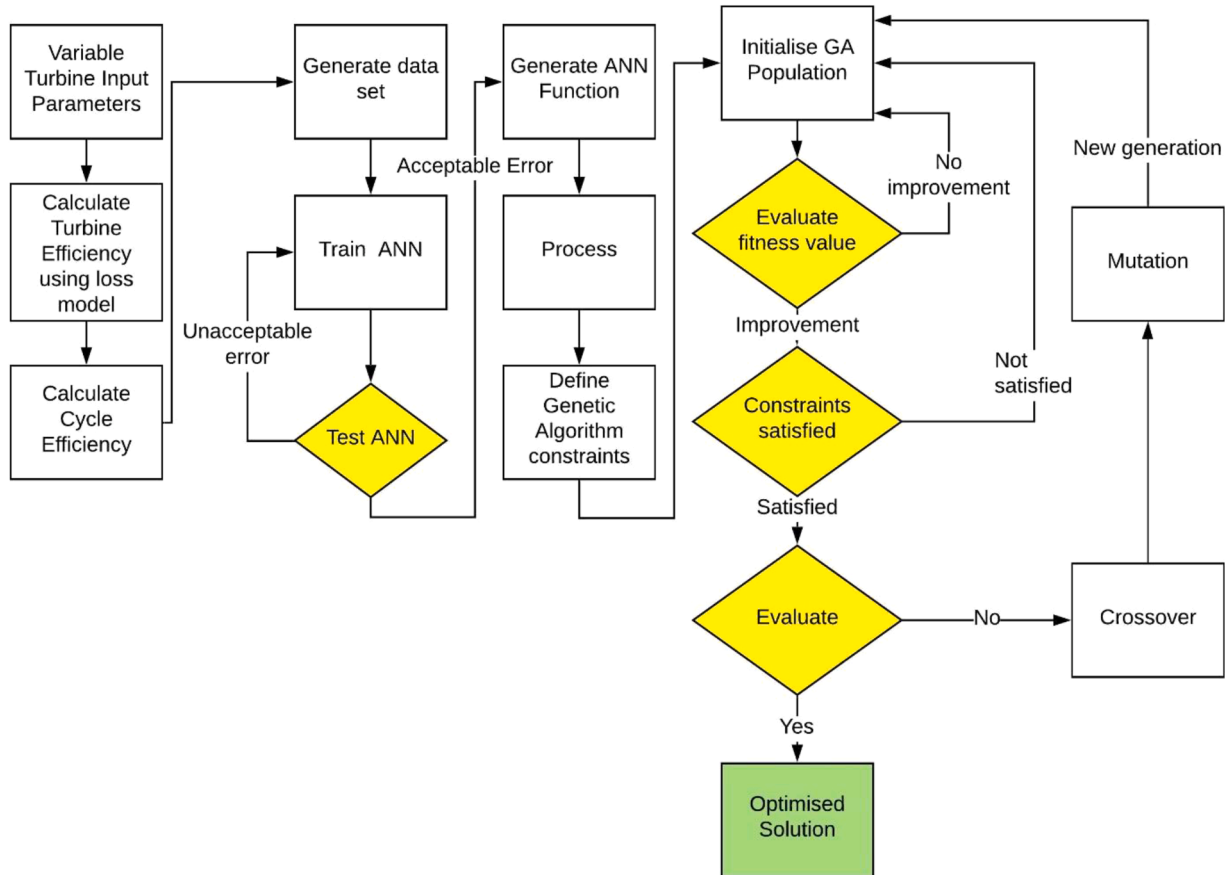


Fig. 3. The layout of an optimization procedure

manufacturing process. Gearbox and Generator losses were ignored [54]. Although the feed pump efficiency was assumed as 70%. The work done by the pump was ignored for determining cycle efficiency, as it was negligible compared to the turbine work [55].

#### 2.4. Deep learning and optimization

Using conventional modeling approaches to optimize the turbine design is computationally intensive. The interrelated parameters that are strongly correlated to the turbine design are the aerodynamic losses, pressure ratio, flow coefficient, stage-loading coefficient, blade velocity, exit angles across the flow path, enthalpy drops across the turbine, and Mach numbers. Therefore, a black-box model based on ANN was developed to correlate the turbine design parameters and the overall cycle efficiency, which subsequently coupled with a GA to optimize the turbine design globally. Fig. 2 shows the connection between the input, hidden, and output layers of the ANN. Fig. 3 presents the integration between ANN and GA.

In this study, 210 trials were generated from the developed 3D flow path model and employed to develop the neural network; 70% of the data points were used to train the neural network, 15% were used to internally validate the neural network evolution to halt the training when generalization stopped improving, while the remaining 15% were used to verify the developed neural network independency. A dropout rate of 0.8 was utilized, which provided a good balance between refining the existing population and allowing new variants. The network comprised 70 neurons in the hidden layer, exceeding the number of individual non-linear terms in the loss model to avoid underfitting the function. While previous studies used a trial and error method to determine the number of neurons, which was time-consuming and relied on operator experience [56], this study considered many neurons, as neural networks did not suffer from over-specifying the problem. A unipolar log-sigmoid activation function was chosen for the hidden layer owing to its robustness [57]. Bayesian Regularization algorithm was employed to train the network due to its robustness for quantitative studies, demonstrating the highest correlation coefficient between predicted and actual data sets [58]. The GA was employed to determine the global optimal design parameters of the axial flow turbine within the predefined constraints (Table 1).

### 3. Results and discussion

#### 3.1. Predictive models verification

The results predicted by numerical Craig and Cox and ANN black-box models were benchmarked against their actual values measured during the steady operation of an existing 450 kW axial-flow impulse back-pressure steam turbine manufactured by IB Turbo – India (Fig. 4). The turbine consisted of 40 stationary nozzles along with 221 moving blades. The nozzle exit metal angle was maintained as 20°. The moving blade metal inlet and exit angles was machined at 22.5° and 19° to the tangential axis. The nozzles had mean pitch, height, throat width and

**Table 1**

Turbine optimization constraints for Genetic Algorithm

Parameter	Lower constraint	Upper constraint
Speed (in RPM) [59]	2000	7000
Hub diameter [59]	0.1	0.7
Degree of reaction [60]	0.0	0.5
Nozzle exit angle [61]	12	20
Nozzle throat [62]	0.003	0.01
Blade throat [62]	0.002	0.01
Nozzle pitch [63]	0.01	0.04
Blade pitch [63]	0.015	0.04
Nozzle backbone length [20]	0.02	0.1
Blade backbone length [20]	0.02	0.1

exit area of 12.4 mm, 42.7 mm, 40.6 mm and 64.1 mm<sup>2</sup> respectively. The turbine mean diameter is 336.55 mm, operated at 9000 rpm, integrated with an alternator through a gearbox. The Turbine was rated for 6.38 kg/sec of mass flow rate, steam inlet conditions up to 15 Kg/cm<sup>2</sup> and 330°C, while steam exhaust pressure was limited to maximum of 9 Kg/cm<sup>2</sup>. Total-to-static turbine efficiency was modelled to within 3% deviation using the Craig and Cox loss model, meaning good agreement with the actual values at multiple load points, as in Table 2.

#### 3.2. Effect of turbine inlet temperature

To study the influence of the inlet temperature on the turbine and cycle performances, the loss models were incorporated into a 1D model for a superheated ORC cycle, shown in Fig. 1. The turbine inlet temperature was between 110°C and 160°C to ensure that the working fluids are in superheated condition. Turbine inlet and outlet pressure were maintained at 15 Kg/cm<sup>2</sup> and 4 Kg/cm<sup>2</sup> respectively. As shown in Fig. 5a, total-to-static turbine efficiency showed an improvement in all fluids except for R600. The improvement in turbine efficiency for R245fa, R1233zd(E), R1234ze(Z), R1234ze(E) and R1234yf were 11.1%, 11.7%, 8.4%, 4.1% and 3.8% respectively. The combined effect of the increased inlet fluid enthalpy and variable turbine efficiency increased the power output by up to 36% (Fig. 5b). Using R245fa, R1233zd(E) and R1234ze(Z) working fluids demonstrated improved cycle efficiency, whereas R1234yf, R1234ze(E), and R600 demonstrated a reduction in cycle efficiency with increased superheat (Fig. 5c). R245fa, R1233zd(E) and R1234ze(Z) experienced the least drop in internal energy across the turbine, which was noted by their lowest power output, as shown in Fig. 5b. The low outlet isentropic Mach numbers, by up to 8% for these fluids, led to a lower isentropic heat drop (Fig. 5d).

Furthermore, the U/C<sub>2</sub> ratios observed for R245fa, R1233zd(E) and R1234ze(Z) were on average 18% higher than those for other fluids (Fig. 5e). On the other hand, the flow coefficients were lowest for these 3 fluids, as shown in Fig. 5f, which is well-aligned with the literature [59]. From the results, it can be concluded that using a multistage, higher rotational speed, or a larger diameter turbine is highly recommended for R600, R1234yf, and R1234ze(E) to maximize turbine efficiency for such fluids.

To understand the contradicting trend of turbine efficiency for R600 fluid, the breakdown of individual losses was investigated. The overall turbine loss consists of the primary and secondary losses for the nozzles and blades. Fig. 6 shows the distribution of the loss factors for all working fluids into the turbine stage for all fluids within the temperature range of 110 - 160 °C. The primary blade loss in R600 increased by 6.1%, compared to 1.7%, 1.48%, 2.62%, 2.59%, and 2.6% for R245fa, R1233zd(E), R1234ze(Z), R1234yf, and R1234ze(E), respectively. This can be attributed to the moving blade profile, the fluid velocity, the high enthalpy drops, and the low molar mass.

The moving blade has a slightly converging flow path across its length, limiting the velocity drop across the profile (Fig. 7). At supersonic flow, the converging fluid path results in a further increase in velocity. Thus, while all other fluids operated at subsonic or transonic conditions, R600 operated at supersonic conditions, as the convergent flow path compounded the fluid velocity.

As fluid velocity was higher for R600, the fluid experienced higher localized velocities at the suction surface. The incremental profile loss generated was applicable for Mach numbers higher than 0.7 and pitch-to-suction surface ratios lower than 0.7 [20]. The enthalpy drop across the turbine is relatively higher in the case of R600. The enthalpy drop is a function of internal energy. The drop in internal energy across the investigated turbine was 77.6 Joules for R600; while R245fa, R1233zd (E), R1234ze(E), R1234ze(Z), and R1234yf, the internal energy drop was 33.4, 33.5, 39.7, 37.2, and 38.9 Joules, respectively. It meant a greater magnitude of conversion from internal to kinetic energy, maintaining the fluid at supersonic conditions and resulting in proportionately greater Mach number loss.

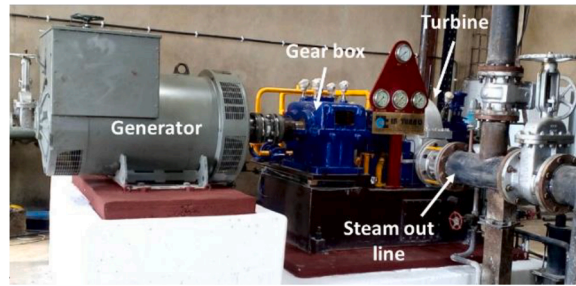


Fig. 4. Pictorial view of the simulated steam turbine operates in a rice mill firm at Karnal, India (permission granted for image)

Table 2  
Modelling verification results

Thermodynamic parameters		Experimental data			Craig & cox model			ANN		
		Load 1	Load 2	Load 3	Load 1	Load 2	Load 3	Load 1	Load 2	Load 3
INPUT	Inlet Pressure (Kg/cm <sup>2</sup> )	10.5	14.4	9.44	10.5	14.4	9.44	10.5	14.4	9.44
	Inlet temperature (°C)	296	311	295	296	311	295	296	311	295
	Outlet Pressure (Kg/cm <sup>2</sup> )	7.8	8.7	6.6	7.8	8.7	6.6	7.8	8.7	6.6
	Mass Flow rate (Kg/cm <sup>2</sup> )	6.11	3.32	5.36	6.11	3.32	5.36	6.11	3.32	5.36
Total-to-static stage efficiency (%)		89.76	90.12	86.44	92.46	92.68	89.38	88.5	89.41	87.17
Static enthalpy after Nozzle (KJ/kg)		2981	2957	2980	2971	2950	2967	2972	2952	2967
Pressure after nozzle (Kg/cm <sup>2</sup> )		8.12	9.1	6.88	8.101	9.1	6.87	7.86	8.7	6.6
Stagnation enthalpy after stage (KJ/kg)		2979	2951	2965	2968	2947	2962	2975	2952	2964
Exit temperature (°C)		263.25	252	258.1	252.9	250.5	253.8	261.7	252.4	254.8
Power output corrected for gearbox and generator efficiency (KW)		396	372	407	408.4	381	419.3	391	368	410

Generally, it is not uncommon to operate in the supersonic regime because of their low molar mass; this was more significant in R600 due to its relatively lower molar mass of 58.12 g/mol. The molar mass of R245fa, R1233zd(E), R1234ze(E), R1234ze(Z) and R1234yf are 134.04, 130.5, 114.04, 114.04, and 114.0 g/mol, respectively [39]. The correlation between these factors is shown in equations 13 and 14.

$$M = \frac{u}{c} \quad (13)$$

$$c = \sqrt{\gamma T \frac{\bar{R}}{MM}} \quad (14)$$

$\bar{R}$  and  $MM$  denote the universal gas constant and the molar mass of the fluid.

Contradictory to the consensus that superheating causing a loss in ORC efficiency [12-16, 64], it was observed that superheating of the working fluid could lead to improved cycle efficiency when used with high molecular mass fluids converging blade profiles and subsonic fluid velocities. The turbine efficiency varied between 66 and 83% (Fig. 5a). This revealed that the working fluid properties and the turbine's design configuration are interrelated. Thus, it reflects the importance of considering the loss model at the component and cycle levels.

### 3.3. Effect of turbine pressure ratio

The effect of varying the pressure ratio on the turbine's efficiency was investigated by varying the turbine inlet pressure ratio between 3 and 10. The turbine inlet temperature was maintained constant at 140 °C. The additional enthalpy drop across the turbine led to a more effective temperature drop (Fig. 8). Although the turbine efficiency demonstrated a significant improvement up to a pressure ratio of 6, the benefits were less significant beyond that, as shown in Fig. 9. The power generated at pressure ratios above 6 was at limited efficiency (Fig. 10). For R600, increasing the pressure ratio reduces the turbine efficiency, as the energy losses in the form of heat are relatively higher when compared to other fluids. Such heat losses are primarily due to the high flow speed over the turbine blades, which is the work-producing

element in the turbine due to its low molar mass, leading to supersonic flow. Fig. 11 demonstrated improvement in cycle efficiency in all cases by increasing the pressure ratio.

Interestingly, the breakdown of the losses shows a significant increase in total losses beyond the pressure ratio of 6 (Fig. 12). Whereas a proportional increase of loss coefficient of about 4.5 was observed per unit increase in pressure ratio for the nozzle primary losses, the blade primary losses demonstrated an exponential two-fold increase beyond the pressure ratio of 6, as shown in Figs 13 and 14, respectively. On the other hand, the change of the secondary losses is marginal with the pressure ratio (Figs 15 and 16).

Detailed investigation of the primary losses demonstrated a direct relationship between the fluid velocity and primary loss coefficients, as shown in Fig. 17 and 18. The Mach number loss was observed to be the most influential on the turbine efficiency. A 44% increase in the nozzle outlet isentropic numbers led to a corresponding 275% increase in the nozzle primary loss coefficient, which indicating conventional profiles experience difficulty undertaking a high expansion ratio [21]; therefore, multistage turbines could be considered for higher pressure ratios, as suggested by Meroni et al. [39]. The additional profile increment loss was a component of the nozzle primary loss, which occurred for values of blade exit isentropic Mach numbers beyond 1.2 [20].

All the investigated fluids, except R600, the moving blade outlet isentropic Mach number demonstrated subsonic fluid velocities up to the pressure ratio of 6. A further increase in pressure ratio led to the operation in the transonic regime. It was observed that increasing the pressure ratio from 3 to 6 led to an average increase of the blade primary loss coefficient by 172% (3.8 units). Increasing the pressure ratio from 6 to 9 increased the blade primary loss coefficient by 191% (11.5 units). Pressure ratios between 3 and 5 demonstrated a reduction in fluid velocity, indicating that the given turbine was best configured for a pressure ratio of 5 for these fluids. On the contrary, R600 demonstrated an increase in total loss coefficient across the entire range of pressure ratio; this is due to the higher moving blade primary and secondary losses resulted from the higher working fluid velocity at the moving blades. These characteristics are shown in Figs 18 and 19.

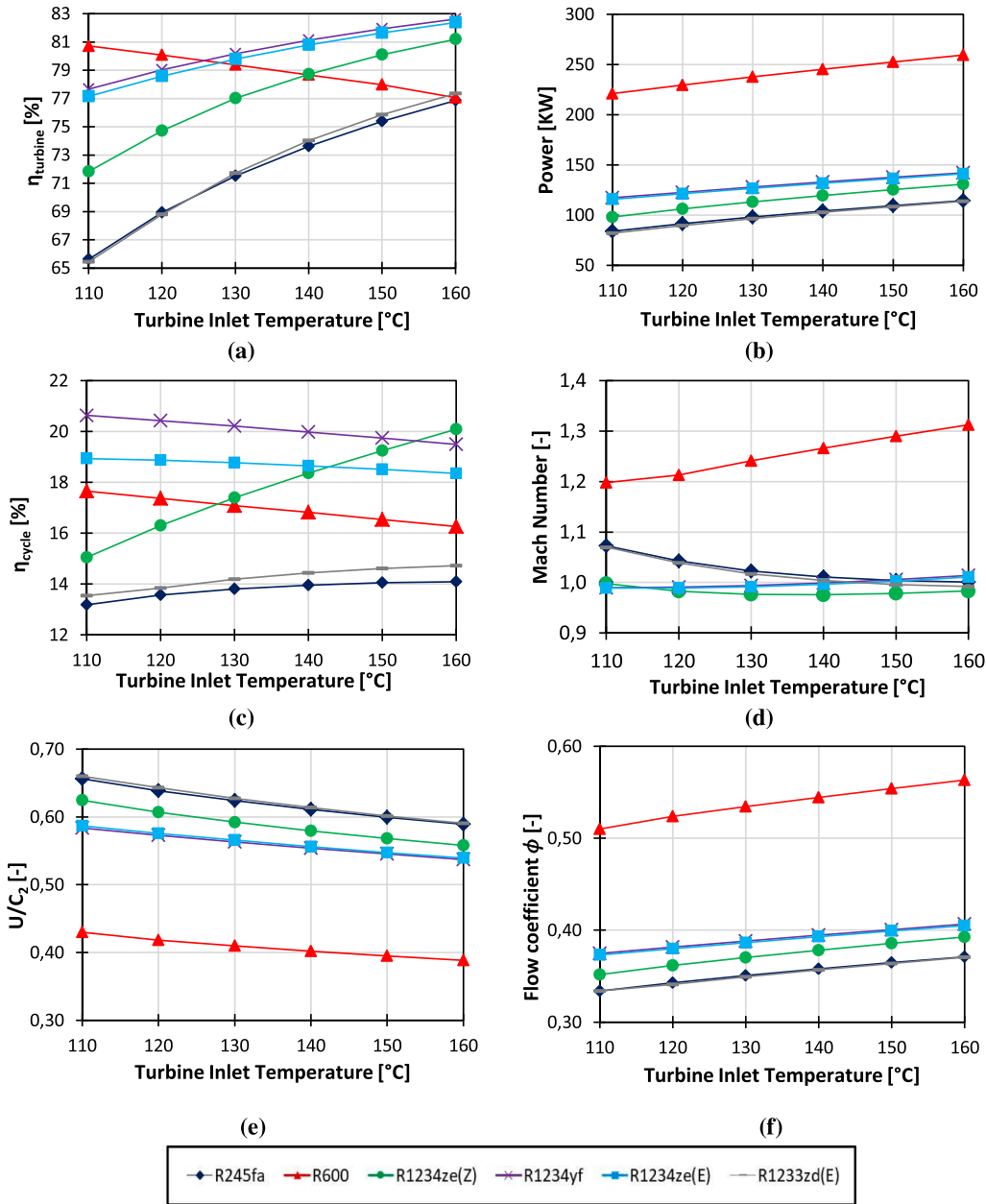


Fig. 5. Influence of inlet temperature on: (a) total to static efficiency, (b) power output, (c) cycle efficiency, (d) relative stage outlet isentropic Mach number, (e)  $U/C_2$  ratio, and (f) flow coefficient

### 3.4. Flow path optimization

The GA was coupled with the ANN turbine model to determine the optimal profile geometry to maximize the turbine's total-to-static efficiency. Given that R1234ze(Z) demonstrated a good total-to-static efficiency for both boundary condition changes (Fig. 5a and Fig. 9), it was considered for optimization. The optimized flow geometrical parameters were verified against the Craig and Cox loss model, as shown in table 3.

It was observed that the optimized profile resulted in a 13.7% improvement in nozzle efficiency at the expense of an 18.9% drop in blade efficiency. As the flow path developed was that of a highly impulse-loaded machine, the algorithm achieved 5.14% higher stage efficiency (Table 4) by compromising blade efficiency for nozzle efficiency. The algorithm increased the degree of reaction, which led to a more evenly distributed enthalpy drop across the nozzle and the moving

blade that led to a 2.6% reduction to nozzle exit velocity ( $C_2$ ) (Table 3). This, in turn, resulted in additional performance gains due to the lower flow coefficient and an optimized coefficient.

The backbone radius ratio loss was a function of the pitch to backbone radius ratio. Decreasing the pitch and increasing the backbone length achieved an 8.6% improvement in backbone radius ratio loss. Reduced trailing edge thickness led to a 66% and 28% reduction in the trailing edge thickness increment loss, respectively ( $loss_{sincr_N}$ ,  $loss_{sincr_B}$ ). The nozzle exit angle ( $\alpha_2$ ) was optimized to reduce the axial component of velocity ( $C_{a2}$ ) and associated losses. The backbone radius ratio loss, trailing edge thickness increment loss ( $loss_{sincr_N}$ ,  $loss_{sincr_B}$ ) and axial component nozzle exit velocity ( $C_{a2}$ ) were factors of the primary loss ( $G_{pN}$ ,  $G_{pB}$ ). The optimized blade profile led to a 1% improvement in overall cycle efficiency (Table 3).

The optimized solutions and original solution furnished in Table 4 were in good agreement with the Smith chart. The Smith chart correlates

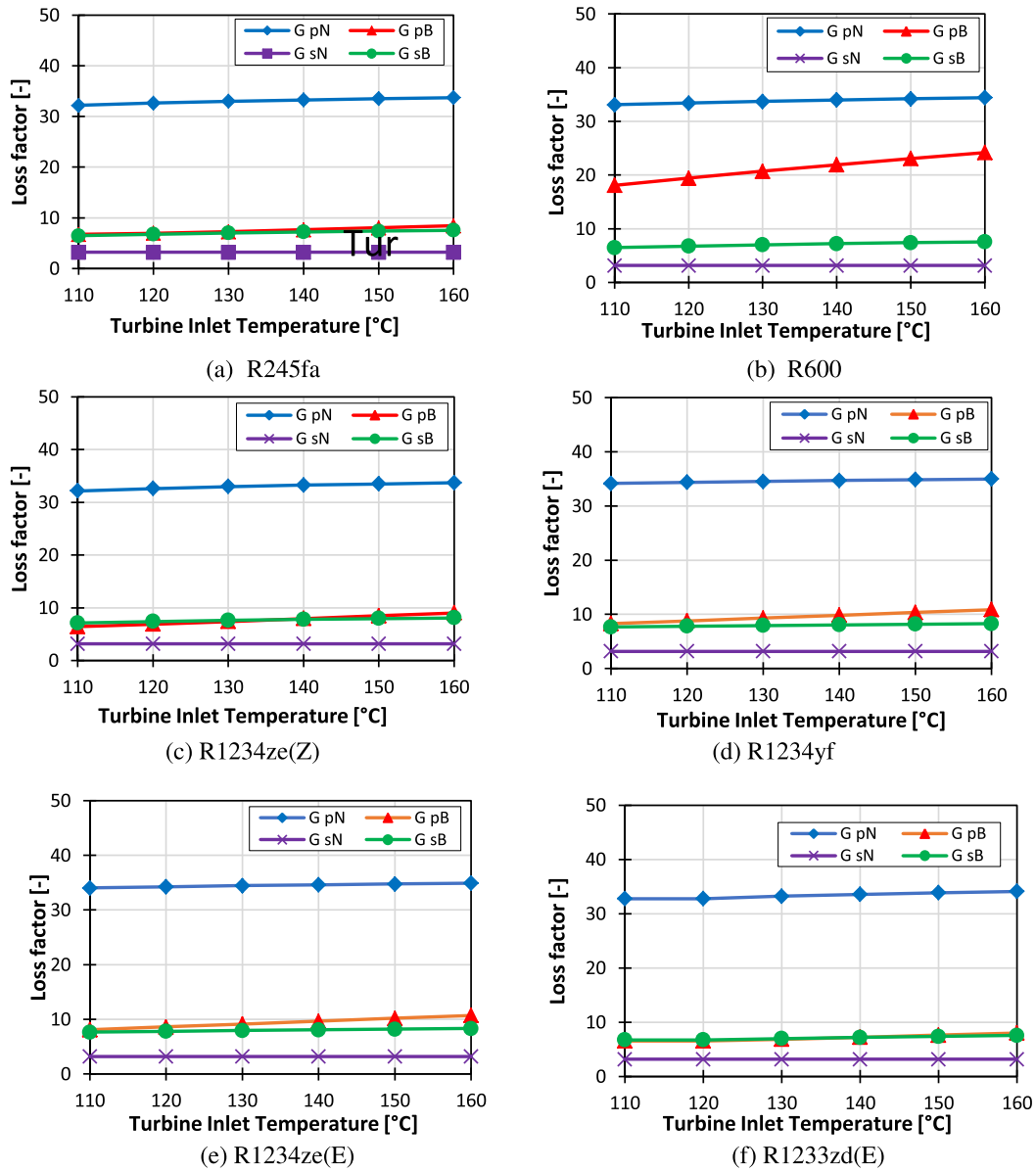


Fig. 6. The influence of turbine inlet temperature on the loss coefficients for the studied fluids

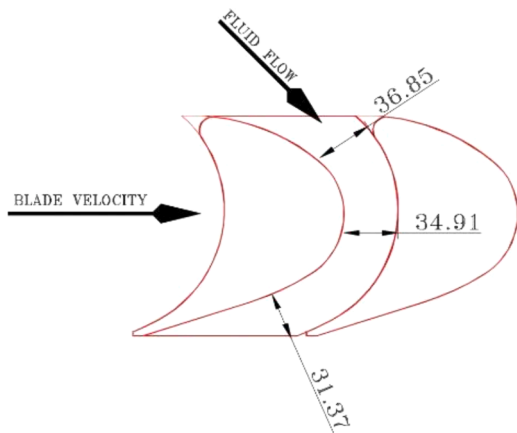


Fig. 7. The converging area of the moving blade section

the turbine efficiency to the flow coefficient ( $\phi$ ) and load coefficient ( $\Psi$ ) [65]. The optimization achieved a 5.2% improvement in total-to-static efficiency. This study showed that the optimized geometrical parameters reduced the flow coefficient ( $\phi$ ) to maximise efficiency, which is in agreement with Turner et al. [65]. Table 5 presents the range of independent variables demonstrating the 98<sup>th</sup> percentile results for the best total-to-static efficiency.

#### 4. Conclusion

This study aimed to envisage the cause of the turbine efficiency losses in the small-scale axial flow turbines and their impact on ORC performance. The direct loss model of Craig and Cox was employed to imitate a small-scale axial flow turbine and integrated it with a 1D model of an Organic Rankine cycle. The ANN coupled with GA was utilized to optimize the turbine flow path and study its influence on the ORC performance and understand the influence of turbine inlet flow conditions and total-to-static stage pressure ratio on the turbine and cyclic performance utilizing a range of organic fluids. The main findings of the current study are summarized below:

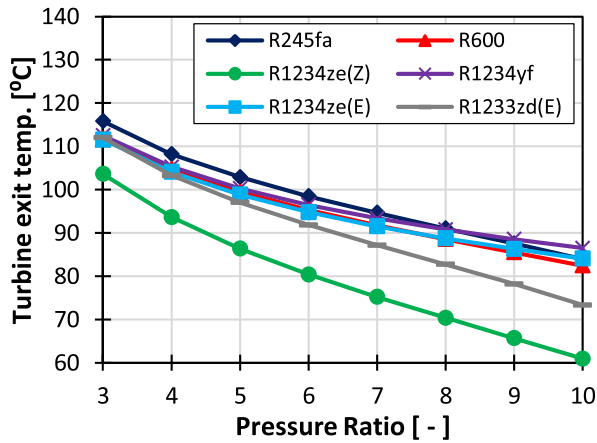


Fig. 8. Exhaust temperature reduction with increasing pressure ratio

- Considering variations in superheat and pressure ratios, the choice of working fluid has a significant impact on cycle design. Higher temperature working fluids, with a higher isentropic drop and lower molar mass are less suitable for conventional single-stage turbine designs, as they lead to approximately 30% higher fluid velocities, as observed in the case of R600.
- Although superheating led to an increase in Mach number loss and blade back radius ratio loss, turbine efficiency improved for most of the investigated organic fluids, with a maximum 12.4% improvement in turbine efficiency in the case of R245fa, R1233zd(E), and R1234ze(Z). Cycle efficiency demonstrated an improvement in the

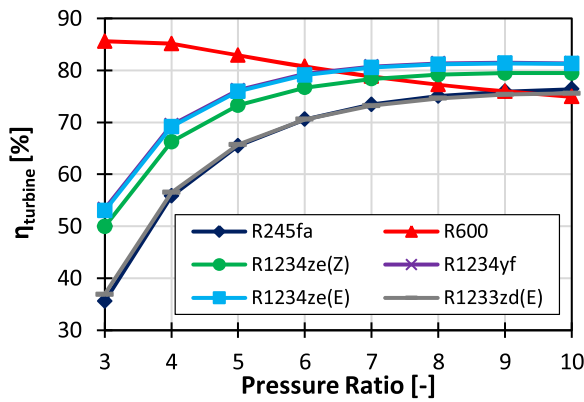


Fig. 9. Variation of total-to-static efficiency with increased pressure ratio

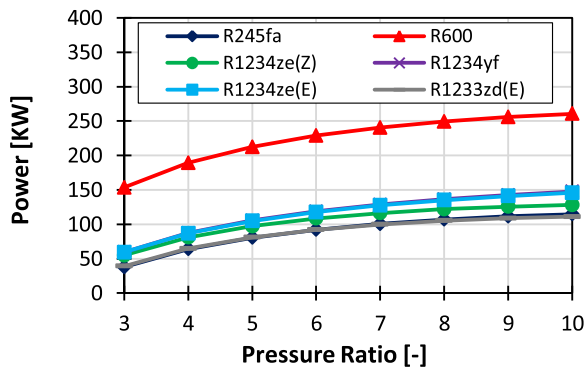


Fig. 10. Non-linear variation of power output with increased pressure ratio

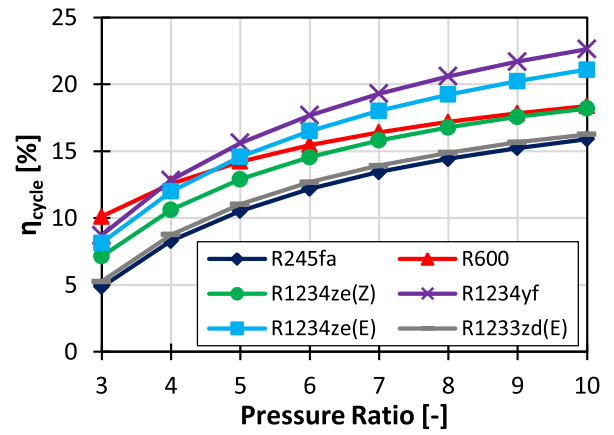


Fig. 11. Improvement in cycle efficiency observed with increased pressure ratio

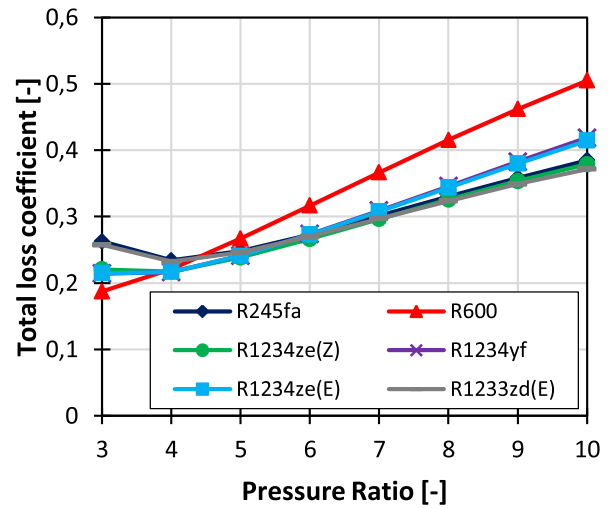


Fig. 12. Variation of total loss coefficient with pressure ratio

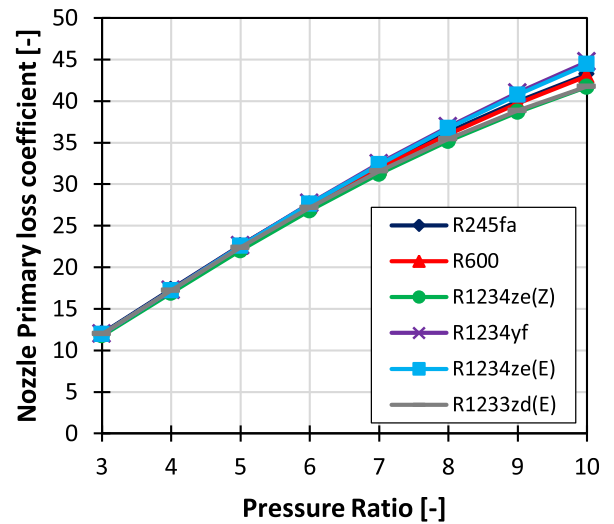


Fig. 13. Variation of nozzle primary loss coefficient with pressure ratio

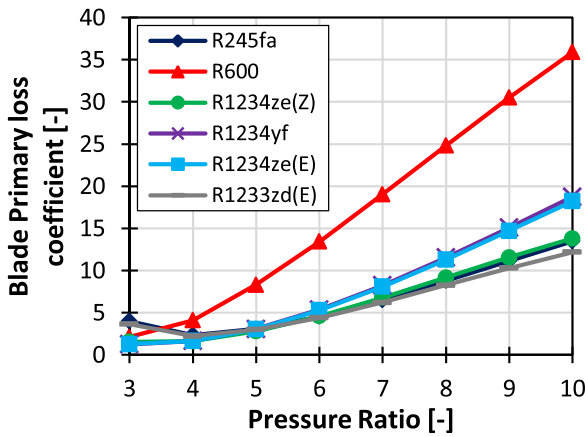


Fig. 14. Variation of blade primary loss coefficient with pressure ratio

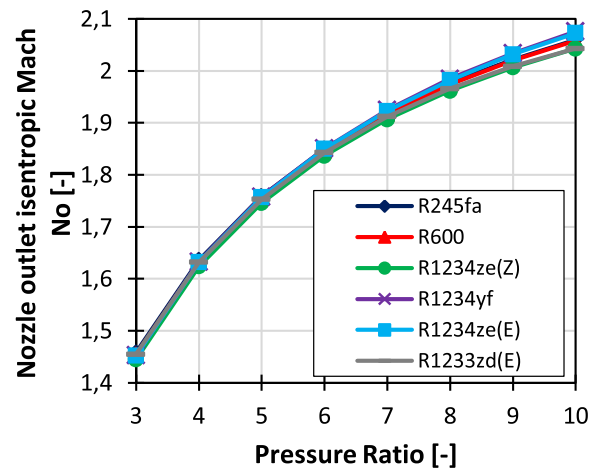


Fig. 17. Variation of nozzle outlet isentropic Mach Number with pressure ratio

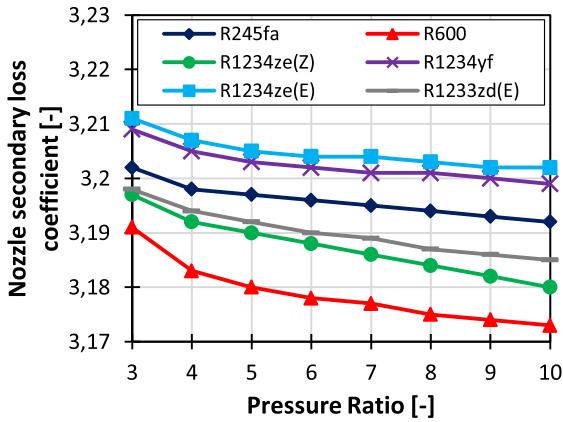


Fig. 15. Variation of nozzle secondary loss coefficient with pressure ratio

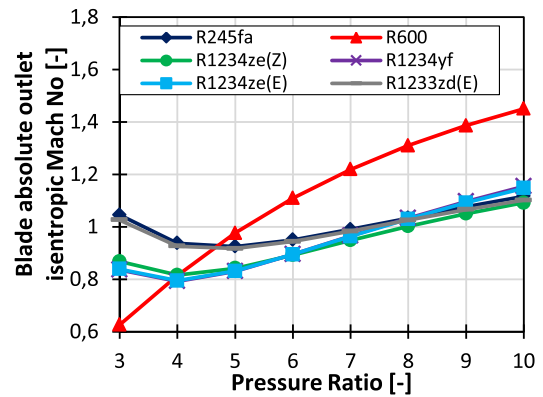


Fig. 18. Variation of blade outlet isentropic Mach no. with pressure ratio

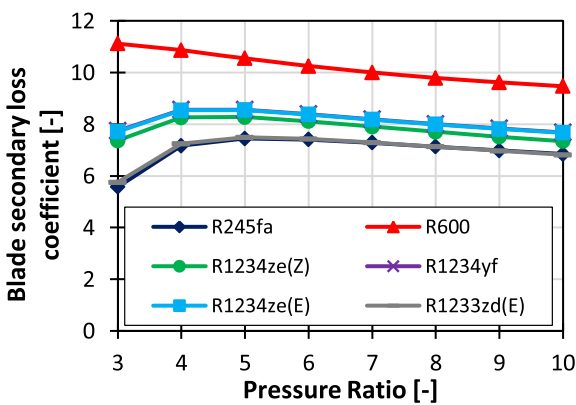


Fig. 16. Variation of blade secondary loss coefficient with pressure ratio

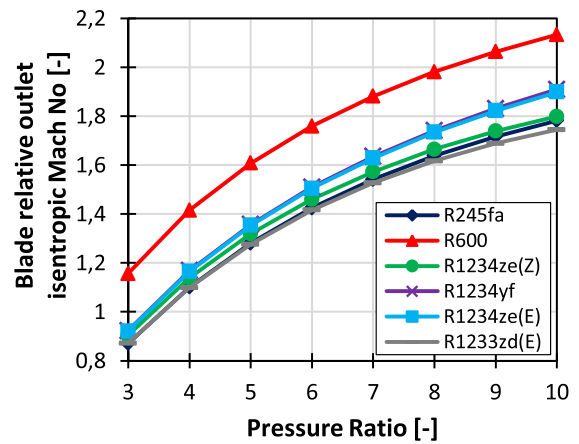


Fig. 19. Variation of blade relative outlet isentropic Mach no. with pressure ratio

**Table 3**  
Genetic Algorithm optimized parameters and test results

Variable type	Parameter	Original value from loss model	GA Optimized values	GA Optimized values verified by Loss model	
<b>Independent Variable</b>	Speed (rpm)	5000	4715.31	4715.31	
	Hub diameter	0.660	0.630	0.630	
	Degree of reaction	0	0.07	0.07	
	Nozzle exit angle ( $\alpha_2$ )	14	12.23	12.23	
	Nozzle throat ( $thr_N$ )	0.004978	0.0065	0.0065	
	Blade throat ( $thr_B$ )	0.00353	0.0061	0.0061	
	Nozzle pitch	0.0294	0.023	0.023	
	Blade pitch	0.01123	0.025	0.025	
	Nozzle backbone length	0.07364	0.0792	0.0792	
	Blade backbone length	0.0217	0.0792	0.0792	
	<b>Dependent Variable</b>	$u$	172.7	162.8	162.8
		$C_2$	281.6	281.83	274.4
		$u/C_2$	0.61	0.57	0.59
		$C_{a2}$	68.11	59.87	58.21
		Total to static efficiency	0.788	0.81	0.84
		Total to total efficiency	0.89	0.93	0.92
		Cycle efficiency	8.78	9.75	9.53
Power		119.5	141.87	123.1	
Volume ratio		7.45	7.34	7.5	
Flow coefficient ( $\varphi$ )		0.37	0.20	0.35	
Load coefficient ( $\Psi$ )		1.32	2.06	1.62	
$G_{pN}$		33.2	30.56	28.84	
$G_{pB}$		7.95	6.40	8.34	
$G_{sN}$		3.16	2.15	2.55	
$G_{sB}$		7.79	8.08	10.38	
$G_{total}$		0.31	0.33	0.30	
$lossincr_N$		0.0099	0.0034	0.0037	
$lossincr_B$	0.0077	0.0057	0.0058		
$M_{detN}$	10.34	31.83	16.6		
$M_{detB}$	19.95	24.52	14.48		
$\Delta X_{pseN}$	17.48	9.39	10.3		
$\Delta X_{pseB}$	5.785	5.294	5.414		

**Table 4**  
Comparison of losses optimized by ANN and GA

Losses	Original	Optimized	Loss reduction in %
Total losses	0.311	0.2951	5.14%
Total nozzle group 1 loss	0.218	0.193	11.5%
Total blade group 1 loss	0.093	0.102	-9.67%
Nozzle primary loss $G_{pN}$	33.22	28.84	13.18%
Nozzle secondary loss $G_{sN}$	3.16	2.55	19.3%
$lossincr_N$	0.0099	0.00375	62%

case of R245fa, R1233zd(E) and R1234ze(Z), which implied that superheated ORC cycles could be beneficial but need to account for variations in turbine efficiency.

- Increasing pressure ratios led to an average 38% increase in turbine efficiency for R245fa, R1234ze(Z), R1234yf, and R1234ze(E). The Mach number of the working fluid, which reached 2.1 at the moving

**Table 5**  
Range of parameter variation provided by optimized solutions

Parameter	Unit	Lower value	Upper value
Turbine speed	rpm	4500	5200
Degree of reaction	-	0.05	0.1
Hub diameter	m	0.5	0.6
Nozzle exit angle	deg	12.5	14
Nozzle throat	mm	6.490	6.511
Blade throat	mm	6.089	6.177
Nozzle pitch	mm	22.807	23.779
Blade pitch	mm	25.211	26.007
Nozzle backbone length	mm	71.439	90.471
Blade backbone length	mm	71.439	90.471

blade, was noted as the most influential on the primary losses. Moving blade relative velocity above 1.6 led to a drastic increase in primary loss, which nullified improvement to turbine efficiency achieved by higher pressure ratios.

- Using deep learning for profile optimization offered a simple and computationally efficient approach for optimizing the flow path's design. The optimized flow path showed a 5.2% improvement in turbine total-to-static efficiency and a 0.24% improvement in cycle efficiency. High percentile results generated by ANNs can be used as a good starting point for advanced blade design.

Consideration of variable turbine efficiency is advisable even for preliminary cycle level design studies, particularly for Superheated ORC cycles. Direct loss models are preferred to help break down the losses to its components. It is recommended to undertake further studies on small-scale ORCs with a lower working fluid molar mass employing multistage turbines. Further development might be needed to widespread machine learning predictive tools as an alternative to Computationally intensive CFD modeling in various applications incorporating a combined turbine and cycle efficiency optimization.

**Author Contributions**

- Yohan Engineer has contributed to developing the turbine model code, completed the results for the paper, developed the initial draft, and worked on the revisions.
- Ahmed Rezk and Abul Kalam Hossain provided guidance and feedback on the overall research and manuscript writing as supervisors for the project.

**Funding**

This research did not receive any specific grant from funding agencies in the public, commercial, or not-for-profit organization.

**Declaration of Competing Interest**

The authors declare that they have no conflict of interest.

**Supplementary materials**

Supplementary material associated with this article can be found, in the online version, at [doi:10.1016/j.ijft.2021.100119](https://doi.org/10.1016/j.ijft.2021.100119).

**References**

- [1] B.K. Bose, Global Warming: Energy, Environmental Pollution, and the Impact of Power Electronics, *IEEE Industrial Electronics Magazine* 4 (1) (2010) 6–17.
- [2] A.Ç. Kone, T. Buks, Forecasting of CO2 emissions from fuel combustion using trend analysis, *Renewable and Sustainable Energy Reviews* 14 (9) (2010) 2906–2915.
- [3] H. Jouhara, et al., Waste heat recovery technologies and applications, *Thermal Science and Engineering Progress* 6 (2018) 268–289.
- [4] A.W. Crook, Profiting from low-grade heat: thermodynamic cycles for low-temperature heat sources, *IET*, 1994.

- [5] U.S.D.o. Energy, Energy use, loss and opportunities analysis: US manufacturing and mining, DOE/ITP, 2004.
- [6] B. Egilegor, et al., ETEKINA: Analysis of the potential for waste heat recovery in three sectors: Aluminium low pressure die casting, steel sector and ceramic tiles manufacturing sector, *International Journal of Thermofluids* 1-2 (2020), 100002.
- [7] D. Brough, H. Jouhara, The aluminium industry: A review on state-of-the-art technologies, environmental impacts and possibilities for waste heat recovery, *International Journal of Thermofluids* 1-2 (2020), 100007.
- [8] T.C. Hung, T.Y. Shai, S.K. Wang, A review of organic rankine cycles (ORCs) for the recovery of low-grade waste heat, *Energy* 22 (7) (1997) 661–667.
- [9] J.J. Fierro, et al., Evaluation of waste heat recovery technologies for the cement industry, *International Journal of Thermofluids* 7-8 (2020), 100040.
- [10] Weiß, A.P. Volumetric expander versus turbine—which is the better choice for small ORC plants.
- [11] R. Rayegan, Y.X. Tao, A critical review on single component working fluids for Organic Rankine Cycles (ORCs), *ASME Early Career Tech. J.* 8 (1) (2009) 20–21.
- [12] Y. Dai, J. Wang, L. Gao, Parametric optimization and comparative study of organic Rankine cycle (ORC) for low grade waste heat recovery, *Energy Conversion and Management* 50 (3) (2009) 576–582.
- [13] K.A. Barse, M.D. Mann, Maximizing ORC performance with optimal match of working fluid with system design, *Applied Thermal Engineering* 100 (2016) 11–19.
- [14] Datla, B.V. and J.J. Brasz, Comparing R1233zd and R245fa for low temperature ORC applications. 2014.
- [15] H.D.M. Hettiarachchi, et al., Optimum design criteria for an organic Rankine cycle using low-temperature geothermal heat sources, *Energy* 32 (9) (2007) 1698–1706.
- [16] R. Chacartegui, et al., Alternative ORC bottoming cycles FOR combined cycle power plants, *Applied Energy* 86 (10) (2009) 2162–2170.
- [17] H. Tian, et al., Fluids and parameters optimization for the organic Rankine cycles (ORCs) used in exhaust heat recovery of Internal Combustion Engine (ICE), *Energy* 47 (1) (2012) 125–136.
- [18] J. Song, C.-w. Gu, X. Ren, Influence of the radial-inflow turbine efficiency prediction on the design and analysis of the Organic Rankine Cycle (ORC) system, *Energy Conversion and Management* 123 (2016) 308–316.
- [19] M.T. White, A.I. Sayma, Simultaneous cycle optimisation and fluid selection for ORC systems accounting for the effect of the operating conditions on turbine efficiency, *Frontiers in Energy Research* 7 (2019) 50.
- [20] H.R.M. Craig, H.J.A. Cox, Performance estimation of axial flow turbines, *Proceedings of the Institution of Mechanical Engineers* 185 (1) (1970) 407–424.
- [21] E. Macchi, A. Perdichizzi, Efficiency prediction for axial-flow turbines operating with nonconventional fluids, *Journal of engineering for power* 103 (4) (1981) 718–724.
- [22] C. Hall, S.L. Dixon, Fluid mechanics and thermodynamics of turbomachinery, Butterworth-Heinemann, 2013.
- [23] A. Lazzaretto, G. Manente, A new criterion to optimize ORC design performance using efficiency correlations for axial and radial turbines, *International Journal of Thermodynamics* 17 (3) (2014) 192–200.
- [24] G. Angelino, M. Gaia, E. Macchi, Medium temperature 100 kW ORC engine for total energy systems, in *Energy Conservation in Industry—Combustion, Heat Recovery and Rankine Cycle Machines*, Springer, 1983, pp. 177–189.
- [25] Lozza, G., E. Macchi, and A. Perdichizzi. On the influence of the number of stages on the efficiency of axial-flow turbines. *American Society of Mechanical Engineers Digital Collection*.
- [26] P. Klonowicz, et al., Significance of loss correlations in performance prediction of small scale, highly loaded turbine stages working in Organic Rankine Cycles, *Energy* 72 (2014) 322–330.
- [27] G. Lozza, A comparison between the Craig-Cox and the Kacker-Okapuu methods of turbine performance prediction, *Meccanica* 17 (4) (1982) 211–221.
- [28] P.I. Onwuamaeze, Improving Steam Turbine Efficiency: An Appraisal, PIONwuamaeze (2018), *Research Journal of Mechanical Operations* 1 (1) (2018) 24–30.
- [29] Y.A.A. Laouid, et al., Towards improvement of waste heat recovery systems: A multi-objective optimization of different organic Rankine cycle configurations, *International Journal of Thermofluids* 11 (2021), 100100.
- [30] S.P. Malysenko, A.I. Schastlivtsev, Thermodynamic efficiency of geothermal power stations with hydrogen steam superheating, *Thermal engineering* 57 (11) (2010) 931–936.
- [31] U. Drescher, D. Brüggemann, Fluid selection for the Organic Rankine Cycle (ORC) in biomass power and heat plants, *Applied Thermal Engineering* 27 (1) (2007) 223–228.
- [32] T. Yamamoto, et al., Design and testing of the Organic Rankine Cycle, *Energy* 26 (3) (2001) 239–251.
- [33] A.P. Weiß, et al., Experimental characterization and comparison of an axial and a cantilever micro-turbine for small-scale Organic Rankine Cycle, *Applied Thermal Engineering* 140 (2018) 235–244.
- [34] A. Oyama, M.-S. Liou, S. Obayashi, Transonic axial-flow blade optimization: Evolutionary algorithms/three-dimensional Navier-Stokes solver, *Journal of Propulsion and Power* 20 (4) (2004) 612–619.
- [35] Ö. Öksüz, İ.S. Akmandor, Multi-objective aerodynamic optimization of axial turbine blades using a novel multilevel genetic algorithm, *Journal of Turbomachinery* 132 (4) (2010), 041009.
- [36] Trigg, M.A., G.R. Tubby, and A.G. Sheard, Automatic genetic optimization approach to two-dimensional blade profile design for steam turbines. 1999.
- [37] M.M. Rashidi, et al., Parametric analysis and optimization of regenerative Clausius and organic Rankine cycles with two feedwater heaters using artificial bees colony and artificial neural network, *Energy* 36 (9) (2011) 5728–5740.
- [38] A. Meroni, et al., Combined Turbine and Cycle Optimization for Organic Rankine Cycle Power Systems—Part A: Turbine Model, *Energies* 9 (5) (2016) 313.
- [39] A. Meroni, et al., Optimization of organic Rankine cycle power systems considering multistage axial turbine design, *Applied Energy* 209 (2018) 339–354.
- [40] V. Maizza, A. Maizza, Unconventional working fluids in organic Rankine-cycles for waste energy recovery systems, *Applied Thermal Engineering* 21 (3) (2001) 381–390.
- [41] M. White, A.I. Sayma, The Application of Similitude Theory for the Performance Prediction of Radial Turbines Within Small-Scale Low-Temperature Organic Rankine Cycles, *Journal of Engineering for Gas Turbines and Power* (12) (2015) 137.
- [42] A.A. Lakew, O. Bolland, Working fluids for low-temperature heat source, *Applied Thermal Engineering* 30 (10) (2010) 1262–1268.
- [43] R. Rayegan, Y.X. Tao, A procedure to select working fluids for Solar Organic Rankine Cycles (ORCs), *Renewable Energy* 36 (2) (2011) 659–670.
- [44] P. Petr, G. Raabe, Evaluation of R-1234ze (Z) as drop-in replacement for R-245fa in Organic Rankine Cycles—From thermophysical properties to cycle performance, *Energy* 93 (2015) 266–274.
- [45] S. Eyerer, et al., Experimental study of an ORC (Organic Rankine Cycle) and analysis of R1233zd-E as a drop-in replacement for R245fa for low temperature heat utilization, *Energy* 103 (2016) 660–671.
- [46] D.G. Ainley, G.C. Mathieson, A method of performance estimation for axial-flow turbines, AERONAUTICAL RESEARCH COUNCIL LONDON (UNITED KINGDOM) (1951).
- [47] R.M. Yablouk, E.E. Markovich, L.E. Al'tshuler, The effect of installing a moisture trap before the moving row on the efficiency of a turbine stage, *Teploténergetika* 13 (3) (1966) 38.
- [48] K. Baumann, Some recent developments in large steam turbine practice, *Journal of the institution of electrical engineers* 59 (302) (1921) 565–623.
- [49] Daily, J.W. and R.E. Nece, Chamber dimension effects on induced flow and frictional resistance of enclosed rotating disks. 1960.
- [50] Enkhbayar, S. and J. Tseyen-Oidov. Compared study of operation regime for FB and CFB steam generators with small and medium capacity. *IEEE*.
- [51] J.M.M. De Escalona, et al., Part-load analysis of gas turbine & ORC combined cycles, *Applied Thermal Engineering* 36 (2012) 63–72.
- [52] D. Meinel, C. Wieland, H. Spliethoff, Effect and comparison of different working fluids on a two-stage organic rankine cycle (ORC) concept, *Applied Thermal Engineering* 63 (1) (2014) 246–253.
- [53] J. Sarkar, Generalized pinch point design method of subcritical-supercritical organic Rankine cycle for maximum heat recovery, *Energy* 143 (2018) 141–150.
- [54] Wieland, N. and D. Thimsen. A practical look at assumptions and constraints for steady state modeling of sCO<sub>2</sub> Brayton power cycles.
- [55] J.P. Roy, M.K. Mishra, A. Misra, Parametric optimization and performance analysis of a waste heat recovery system using Organic Rankine Cycle, *Energy* 35 (12) (2010) 5049–5062.
- [56] F. Yilmaz, R. Selbaş, A.Ş. Şahin, Efficiency analysis of organic Rankine cycle with internal heat exchanger using neural network, 52, *Heat and Mass Transfer*, 2016, pp. 351–359.
- [57] B. Karlik, A.V. Olgac, Performance analysis of various activation functions in generalized MLP architectures of neural networks, *International Journal of Artificial Intelligence and Expert Systems* 1 (4) (2011) 111–122.
- [58] M. Kayri, Predictive abilities of bayesian regularization and Levenberg–Marquardt algorithms in artificial neural networks: a comparative empirical study on social data, *Mathematical and Computational Applications* 21 (2) (2016) 20.
- [59] S.F. Smith, A simple correlation of turbine efficiency, *The Aeronautical Journal* 69 (655) (1965) 467–470.
- [60] Moroz, L., et al. Axial turbine flow path design for an organic Rankine cycle using R-245fa. *American Society of Mechanical Engineers*.
- [61] A. Rusanov, R. Rusanov, P. Lampart, Designing and updating the flow part of axial and radial-axial turbines through mathematical modeling, *Open Engineering* 5 (1) (2015).
- [62] H. Moustapha, et al., Axial and radial turbines, 2, Concepts NREC, White River Junction, VT, 2003.
- [63] L. Talluri, G. Lombardi, Simulation and Design Tool for ORC Axial Turbine Stage, *Energy Procedia* 129 (2017) 277–284.
- [64] J.P. Roy, M.K. Mishra, A. Misra, Performance analysis of an Organic Rankine Cycle with superheating under different heat source temperature conditions, *Applied Energy* 88 (9) (2011) 2995–3004.
- [65] Turner, M., A. Merchant, and D. Bruna, Applications of a Turbomachinery Design Tool for Compressors and Turbines. 2007.